

## Density functional theory based study of chlorine doped WS<sub>2</sub>-metal interface

Anuja Chanana and Santanu Mahapatra

Citation: [Applied Physics Letters](#) **108**, 103107 (2016); doi: 10.1063/1.4943267

View online: <http://dx.doi.org/10.1063/1.4943267>

View Table of Contents: <http://scitation.aip.org/content/aip/journal/apl/108/10?ver=pdfcov>

Published by the [AIP Publishing](#)

---

### Articles you may be interested in

[Schottky contacts to In<sub>2</sub>O<sub>3</sub>](#)

APL Mater. **2**, 046104 (2014); 10.1063/1.4870536

[Electrical transport across Au/Nb:SrTiO<sub>3</sub> Schottky interface with different Nb doping](#)

Appl. Phys. Lett. **100**, 213502 (2012); 10.1063/1.4720516

[Electronic structures of an epitaxial graphene monolayer on SiC\(0001\) after metal intercalation \(metal=Al, Ag, Au, Pt, and Pd\): A first-principles study](#)

Appl. Phys. Lett. **100**, 063115 (2012); 10.1063/1.3682303

[n-type doping in Cu<sub>2</sub>O with F, Cl, and Br: A first-principles study](#)

J. Appl. Phys. **111**, 023709 (2012); 10.1063/1.3677989

[Submicron contacts for electrical characterization of semiconducting WS<sub>2</sub> thin films](#)

J. Vac. Sci. Technol. A **16**, 1239 (1998); 10.1116/1.581266

---

The advertisement features a Lake Shore Model 372 cryogenic temperature controller on the left, which is a white rectangular device with a digital display and a keypad. On the right, there is a detailed, artistic rendering of a cryogenic system, showing various components like pipes, valves, and a large cylindrical vessel, all set against a blue background. The text 'Precise temperature control for cryogenic research' is prominently displayed in white, and the 'Lake Shore CRYOTRONICS' logo is in the top right corner.

Precise temperature control  
for cryogenic research

Model 372

Lake Shore  
CRYOTRONICS

## Density functional theory based study of chlorine doped WS<sub>2</sub>-metal interface

Anuja Chanana and Santanu Mahapatra<sup>a)</sup>

*NanoScale Device Research Laboratory, Department of Electronic Systems Engineering, Indian Institute of Science, Bengaluru, Karnataka 560012, India*

(Received 12 October 2015; accepted 23 February 2016; published online 10 March 2016)

Investigation of a transition metal dichalcogenide (TMD)-metal interface is essential for the effective functioning of monolayer TMD based field effect transistors. In this work, we employ the Density Functional Theory calculations to analyze the modulation of the electronic structure of monolayer WS<sub>2</sub> with chlorine doping and the relative changes in the contact properties when interfaced with gold and palladium. We initially examine the atomic and electronic structures of pure and doped monolayer WS<sub>2</sub> supercell and explore the formation of midgap states with band splitting near the conduction band edge. Further, we analyze the contact nature of the pure supercell with Au and Pd. We find that while Au is physisorbed and forms n-type contact, Pd is chemisorped and forms p-type contact with a higher valence electron density. Next, we study the interface formed between the Cl-doped supercell and metals and observe a reduction in the Schottky barrier height (SBH) in comparison to the pure supercell. This reduction found is higher for Pd in comparison to Au, which is further validated by examining the charge transfer occurring at the interface. Our study confirms that Cl doping is an efficient mechanism to reduce the n-SBH for both Au and Pd, which form different types of contact with WS<sub>2</sub>. © 2016 AIP Publishing LLC. [<http://dx.doi.org/10.1063/1.4943267>]

After the fabrication of field effect transistor (FET) using monolayer MoS<sub>2</sub>,<sup>1</sup> the 2D layered transition metal dichalcogenides (TMDs) have garnered enormous attention in the electron devices community. Apart from MoS<sub>2</sub>, other TMDs such as WS<sub>2</sub>,<sup>2,3</sup> WSe<sub>2</sub>,<sup>4</sup> MoSe<sub>2</sub>,<sup>5</sup> and MoTe<sub>2</sub><sup>6</sup> are also explored as channel materials for FETs. In the absence of efficient doping techniques, these transistors exhibit Schottky barrier height (SBH) at the source/drain contact, which leads to a low ON current. Tremendous efforts are dedicated to reduce the contact resistance at the TMD-metal interface by employing different techniques both theoretically and experimentally.<sup>7–12</sup> However, most of these efforts are focused towards MoS<sub>2</sub> and WSe<sub>2</sub>, and a minimum study is devoted to other TMD's-metal contact interfaces. A study using ballistic MOSFET model reveals that WS<sub>2</sub> outperforms all other TMDs.<sup>13</sup> Experimental reports of WS<sub>2</sub> device fabrication<sup>2</sup> and Cl doping technique for reducing WS<sub>2</sub>-metal contact resistance are also reported.<sup>14</sup> However, theoretical investigations of WS<sub>2</sub> metal contact interface using first principles is still lacking in the literature. Since first principles are extensively used to analyze the graphene-metal,<sup>15,16</sup> MoS<sub>2</sub>-metal,<sup>17</sup> and WSe<sub>2</sub>-metal,<sup>18</sup> it is believed that it will efficiently describe the contact nature with other TMDs as well. For WS<sub>2</sub>, chlorine doping, which is done by replacing sulfur atoms, is the first ever method demonstrated experimentally to reduce the WS<sub>2</sub>-contact resistance, exhibiting both high drain current and field-effect mobility.<sup>14</sup> In this work, we employ the density function theory (DFT) to study the electronic structure of the interface between WS<sub>2</sub> and one physisorped (Au) and one chemisorped metal. We then examine the effect of chlorine doping by substituting sulfur atoms to address the SBH mitigation at WS<sub>2</sub>-metal interface.

We start by analyzing the electronic dispersion characteristics of pure and Cl-doped WS<sub>2</sub> and explore the shifts in the energy bands with respect to Fermi level ( $E_f$ ) and further analyze the mid gapstates formed near the conduction band (CB) edge. To preserve the stability in the  $5 \times 5$  WS<sub>2</sub> supercell, the number of chlorine dopants substituting the sulfur atoms is kept one. We perform the formation energy calculations ( $E_{Form}$ ) to find the stability of the chlorine doped structure. Next, this supercell is interfaced with  $\langle 111 \rangle$  cleaved surfaces of Au and Pd, respectively, and the contact nature is studied. The SBH is evaluated using the projected bandstructure and the density of states. The charge transfer across the interface is analyzed using the valence electron density and charge density difference. An electron localization function (ELF) is employed to study the localization of electrons at the WS<sub>2</sub>-metal interface. A thorough examination of all the above analysis leads to a conclusion that n-type doping of WS<sub>2</sub> using chlorine as an effective substitute results in lowering of n-SBH at the WS<sub>2</sub>-metal interface.

We carry out the DFT simulations employing Atomistix Tool Kit (ATK)<sup>19</sup> with Local Density Approximation (LDA)-Perdew Zung (PZ)<sup>20</sup> as the exchange correlation to investigate the WS<sub>2</sub> (pure and doped)-metal (Au and Pd) interfaces. The pseudopotentials of various elements (tungsten, sulfur, chlorine, gold, and palladium) as generated by Hartwingster-Goedecker-Hutter<sup>21</sup> based on the concept of fully relativistic all electron calculation are used for the present study. The orbital contribution in Tier 4 basis set is found to be appropriate for generating the band gap of monolayer WS<sub>2</sub>. It is worth noting that in transition metals (e.g., W and Pd), the overlap between the core and valence electrons is substantial. The commonly used double zeta polarized (DZP) basis function generated using FHI pseudopotential does not consider the semicore electrons and might not yield results of considerable accuracy. On the other hand, the

<sup>a)</sup>santanu@dese.iisc.ernet.in

HGH pseudopotentials include semicore electrons and thus are expected to produce the electronic structure of the TMD-metal interface precisely. However, their usage significantly enhances the computational budget since they require a larger number of basis functions as compared to DZP. The density mesh cut off is 75 Hartree with a Monkhorst Pack k-point<sup>22</sup> sampling of  $9 \times 9 \times 1$  mesh. The convergence criterion of the self-consistent loop is set at a value of  $10^{-5}$  Hartree.

We first confirm the band gap of  $\text{WS}_2$  unit cell and find the value to be 2.07 eV, nearly consistent with the earlier reports.<sup>23,24</sup> A  $5 \times 5$  supercell is formed using the optimized unit cell, which is computationally appropriate to study the doping similar to the one reported here.<sup>25</sup> The interface strain between the pure and doped  $\text{WS}_2$  supercell with  $\langle 111 \rangle$  cleaved surface of gold and palladium is found to be 1.3% and 2.1%, respectively. Doping is achieved by replacing one sulfur atom with a chlorine atom in the supercell, which amounts to 2% of the total sulfur atoms. For evaluating  $E_{Form}$  for sulfur substitution,  $\text{X}_2$  dimers of each  $\text{Cl}_2$  and  $\text{S}_2$  are taken, and then, the total energy of the substitutional atoms and host atoms in the formation energy equation<sup>26</sup> are calculated. Four layers of  $\langle 111 \rangle$  cleaved surface of metal are then interfaced with the  $\text{WS}_2$  supercell and is found relevant to study the  $\text{MoS}_2$ -metal interface.<sup>27</sup> To minimize false interactions between the periodic interfaced geometries, vacuum length of  $20 \text{ \AA}$  is considered. A force optimization of  $(0.001 \text{ eV/\AA})$  is performed for both unit cell and supercell (pure and doped) of the  $\text{WS}_2$  using the limited memory Broyden-Fletcher-Goldfarb-Shannon (LBFGS) method. The volume of the structure is allowed to change using a stress optimization of  $(0.001 \text{ eV/\AA}^{-3})$  in both unit cell and supercell of  $\text{WS}_2$ .

Figure 1(a) shows the stable atomic structure of chlorine doped  $5 \times 5$  supercell of  $\text{WS}_2$ . We perform the formation energy calculations to find the thermodynamically stable position for sulfur substitution by chlorine atoms with the  $E_{Form}$  values as 2.92 eV. This supercell is interfaced with  $\langle 111 \rangle$  cleaved surface of Au and Pd, respectively. While interfacing, the lattice constant of  $\text{WS}_2$  is fixed and the metal slab is subjected to match with it. Figures 1(c) and 1(d) show the ball and stick model of the doped  $5 \times 5$   $\text{WS}_2$ -Au and  $\text{WS}_2$ -Pd interface. The total energy calculations reveal  $2.7 \text{ \AA}$  and  $2.2 \text{ \AA}$  as the equilibrium interlayer separation between the  $\text{WS}_2$  (pure and doped) with Au and Pd metal slabs. The binding energy values obtained per sulfur atom are  $-0.18 \text{ eV}$  (pure) and  $-0.19 \text{ eV}$  (doped) for gold and  $-0.39 \text{ eV}$  (pure) and  $-0.4 \text{ eV}$  (doped) for palladium, respectively. We calculate the work function of the pure and doped  $\text{WS}_2$ , and metals Au and Pd and are shown in Figure 1(f).

Substituting by chlorine doping amounts to 2% of total sulfur atoms, which leads to a very high doping concentration in a  $5 \times 5$  supercell of  $\text{WS}_2$ . However, to realize the substitution by considering the experimental doping concentration value of  $6 \times 10^{11} \text{ cm}^{-2}$  studied here,<sup>14</sup> a much bigger supercell is required, leading to a further increase in computational burden. To reduce the computational cost and study the effect of doping on SBH reduction, we limit ourselves with a  $5 \times 5$  supercell.

The electronic structures of both the pure and doped  $\text{WS}_2$  along with the density of states are compared in Figure 2 to

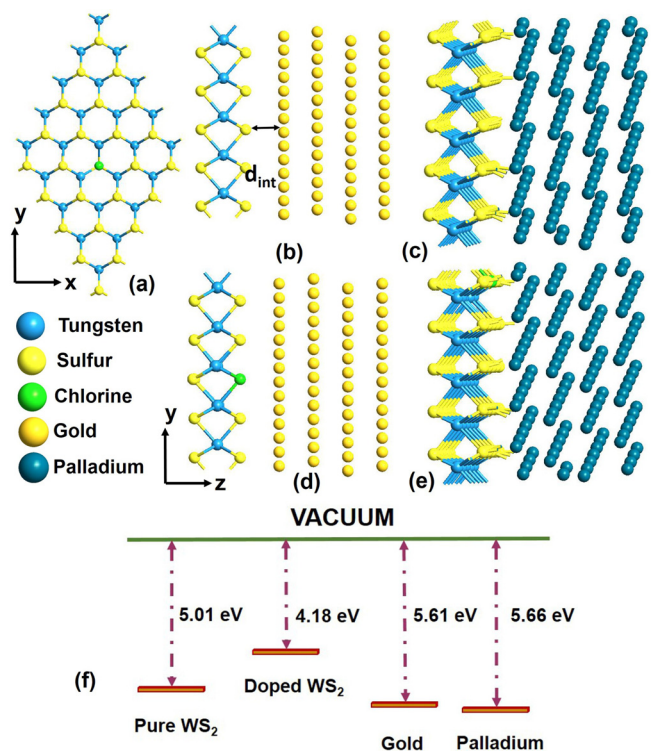


FIG. 1. (a) Chlorine substituted  $5 \times 5$  supercell of  $\text{WS}_2$  presented using the ball-stick model. Atomic model of the pure  $\text{WS}_2$   $5 \times 5$  supercell (b) and (c) and doped supercell (d) and (e) interfaced with  $\langle 111 \rangle$  cleaved surface of face centered cubic (FCC) metals gold and palladium. The configuration is stable when the interlayer distance is  $2.7 \text{ \AA}$  for gold and  $2.2 \text{ \AA}$  for palladium.  $d_{int}$  denotes the equilibrium distance with the minimum binding energy along the z-direction. (f) Work function values of the pure and doped  $\text{WS}_2$  along with the metals Au and Pd calculated using DFT simulations.

highlight the effect of doping. The band gap of pure  $\text{WS}_2$  is 2.07 eV. The positions of CB and Valence Band (VB) are verified with PDOS kept along the side of bandstructure. We see that substituting a single chlorine dopant shifts the energy bands towards the  $E_F$  and creates the midgap states in the vicinity of  $E_F$ . The number of midgap states is 2, one of which splits into two bands between the high symmetry points of Brillouin zone shown in the inset of Figure 2(c). The two midgap states have significant contribution in the PDOS as well. The main contributor of these states is chlorine, which is shown in the inset of Figure 2(d) with purple color. The energy level is 0.184 eV for the midgap state near the conduction band minima (CBM). The splitting of bands leads to two energy levels of 0.028 eV and 0.020 eV, respectively. These defect states originate from the hybridization of the Cl 3p and the W 5d states. There exists one unpaired extra electron due to n-type doping by chlorine. As tungsten lies in the 6th period of the periodic table, chlorine, which has an extra negative charge, leads to the energy splitting of W d-orbitals and thus contributes to an extra midgap state. The band gap in doped  $\text{WS}_2$  is also different as compared to the pure supercell (by 0.05 eV), which is attributed to the hybridization and change in the atomic structure due to chlorine substitution.

We then perform simulations to evaluate the nature of contact formed with  $\text{WS}_2$  (pure and doped) with Au and Pd. The Schottky barrier height is assessed using the electronic structure and DOS of the projected  $\text{WS}_2$ . The valence electron density and charge density difference are used to

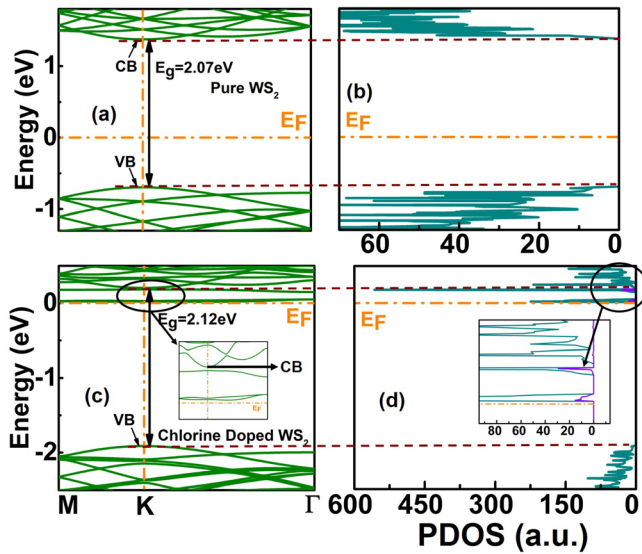


FIG. 2. Projected bandstructure and DOS of (a) and (b) pure  $\text{WS}_2$  and (c) and (d) chlorine doped  $\text{WS}_2$ . PDOS placed along the side verifies the position of CB and VB. Doping with chlorine leads to the appearance of midgap states in the  $\text{WS}_2$  band gap and their contribution is studied using the DOS. The number of midgap states is 2 for doped  $\text{WS}_2$ . The inset in (c) shows the exact position of CBM and the midgap states. The purple line in (d) shows the chlorine contribution in PDOS and is highlighted in the inset. The contribution of midgap states is confirmed by the PDOS, and the peaks in PDOS occur at the same energy level as in the bandstructure. CB, VB,  $E_F$ , and  $E_g$  denotes the conduction band edge, valence band edge, Fermi level and band gap, respectively. Fermi level is at zero energy. The dashed brown lines join the CBM and VBM in the bandstructure and DOS.

estimate the charge transfer across the interface. The localisation of electrons at the  $\text{WS}_2$ -metal interface is studied using the ELF.

Both the p- and n-type SBH of the projected  $\text{WS}_2$  (pure and doped) with Au and Pd are shown in Figures 3(a)–3(d). Since the interface involves two different atomic structures, the nature band gap is lost, and the projected band structure

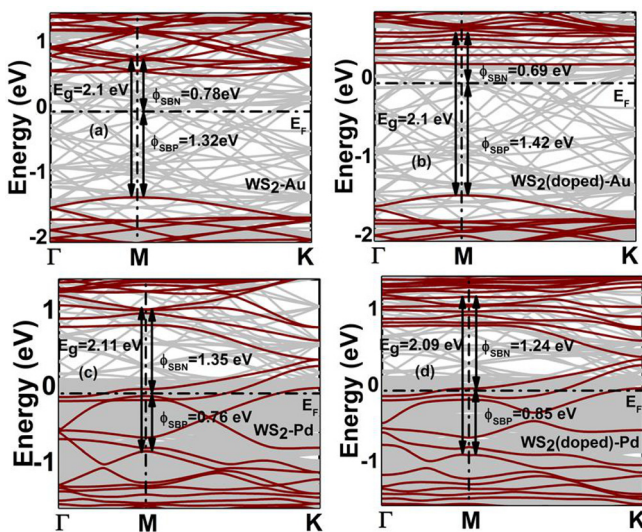


FIG. 3. Projected electronic bandstructure of the  $\text{WS}_2$ -metal (Au and Pd) interface for (a) and (c) pure (b) and (d) doped supercells. The projected bandstructure (wine color lines) is superimposed on the total bandstructure  $\text{WS}_2$ -metal systems (grey lines). Au forms an n-type SB contact whereas Pd forms a p-type SB contact.  $\phi_{SB,P}$  and  $\phi_{SB,N}$  are the p- and n-type Schottky barrier heights.  $E_g$  is the total band gap measured from the CBM and VBM.  $E_F$  is the Fermi level.

comprises of interface states. The origin of these states lies in the complex electronic hybridization occurring at the  $\text{WS}_2$ -metal interface. Au is found to be physisorbed with  $\text{WS}_2$  whereas Pd is chemisorbed. Au, being an s-electron metal, shows less hybridization as compared to Pd, which is a d-electron metal, and this effect is similar to  $\text{MoS}_2$ -metal interface.<sup>27</sup> The binding energy values quoted earlier confirm this nature. Moreover, the band gap regime also consists of less interface states in Au as compared to Pd (Figures 3(a) and 3(c)).

For a pure  $\text{WS}_2$ -Au interface, the amount of complexity in the bandstructure is less, but for a doped interface, it is very high. This happens because the atoms in the doped supercell already hybridize with the substitutional impurity. The difference is visible in Figures 3(b) and 3(d) with respect to Figures 3(a) and 3(c). It further makes the determination of band gap edges difficult. However, the density of states along with the electronic structure of projected  $\text{WS}_2$  can be used to identify the CBM and valence band maxima (VBM), as demonstrated in Ref. 8. The difference between the CBM and VBM of all the interfaces differs from the band gap of pure  $\text{WS}_2$  by 0.04 eV. Strong interface hybridization causes emergence of more midgap states for both the pure and doped supercells as visible in Figures 3(c) and 3(d) for Pd due to its chemisorption nature with  $\text{WS}_2$ . We observe that Au shows an n-type SBH and Pd shows p-type SBH when interfaced with  $\text{WS}_2$ . The values of SBH are 0.78 eV and 0.76 eV, respectively. In the complete band structure shown by grey lines, we see that for Au the band lines are more dispersed in comparison to Pd. This indicates a strong bonding of  $\text{WS}_2$  with Pd. Moreover, below the Fermi level, we see a complete metallization for Pd, leading to the formation of the p-type contact. Here, we see a similarity in the nature of contact between  $\text{WS}_2$  and  $\text{WSe}_2$  while forming an interface with Au and Pd.<sup>18</sup> With the introduction of n-type impurity, the n-SBH exhibits a reduction for both metals. The n-SBH reduction attained is 0.09 eV for Au and 0.11 eV for Pd. We see that the reduction in the n-SBH is higher for Pd in comparison to Au. Pd showing a p-type contact with  $\text{WS}_2$  also exhibits a reduction in the n-SBH and increase in p-SBH. This validates the observation that the chlorine is effective in reducing n-SBH for both the types of metals forming p- and n-type SBH with  $\text{WS}_2$  and is equally competent for chemisorbed and physisorbed metal interface with  $\text{WS}_2$ . A slight variance in the band gap value of  $\text{WS}_2$  2.07 (for pure  $\text{WS}_2$  bandstructure)—2.1 and 2.09 (projected  $\text{WS}_2$  bandstructure) is also observed due to heterogeneous atomic interface.

We also evaluate the valence electron density for the  $\text{WS}_2$ -metal interface, as shown in Figure 4. The value of valence electron density is calculated as the minimum electron density at the metal-semiconductor interface. Higher values of electron density at the interface imply a better electron injection efficiency. The values with Au are for pure  $0.10727 \text{ \AA}^{-3}$  and  $0.10816 \text{ \AA}^{-3}$  for doped supercell. For pure and doped supercell with Pd, they are  $0.21888 \text{ \AA}^{-3}$  and  $0.2212 \text{ \AA}^{-3}$ , respectively. The high values for Pd indicate that more charge transfer has occurred when it is interfaced with  $\text{WS}_2$ . Moreover, the difference in the density values of the doped and pure interface is higher for Pd as compared to those for Au.

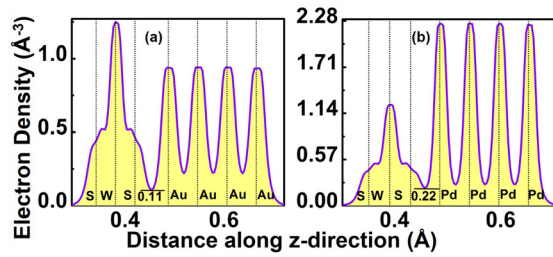


FIG. 4. 1D projection of average valence electron density along the  $z$ -direction for pure (a)  $\text{WS}_2$ -Au and (b)  $\text{WS}_2$ -Pd interface. The value of valence electron density is evaluated between the nearest sulfur atomic layer of  $\text{WS}_2$  and the nearest layer of metal formed at the  $\text{WS}_2$ -metal interface geometry and is shown by black horizontal lines. The position of atoms is shown by black dotted lines.

To substantiate the observations made in the above analysis, we examine the charge density difference of the respective geometries. Figure 5 shows the average charge density difference of the  $\text{WS}_2$ -metal interface for (a) Au and (b) Pd. A dipole gets created at the interface since both accumulation and depletion regions exist. Both the regions are shown by dissimilar colors to highlight the difference between them. At the junction between the nearest sulfur atom and metal atom, two peaks exist for the depletion region and one peak for the accumulation region. Moreover, the accumulation shows a higher charge difference in Pd as compared to Au. A higher depletion regime implies that the charge carriers are repelled back from the surface and evinces a probability of least transmission across the interface. On the other hand, a higher accumulation regime implies that more charge is transferred across the interface. Hence, we observe more hybridization for Pd rather than Au. The area calculated between the nearest S and metal atom using the methodology exhibited in Ref. 8 is  $0.03181 \times 10^{-3}$  for Au and  $0.06031 \times 10^{-3}$  for Pd, respectively, and thus affirms the charge transfer is high for Pd. For the pure and doped supercell-metal interface, the charge density difference curve shows a similar nature and the difference in areas for the pure and doped case is higher for Pd. Because of this difference, a greater reduction in n-SBH is observed in Pd with respect to Au.

To study the localization of electrons at the  $\text{WS}_2$ -metal interface, we study ELF, which is a dimensionless quantity. It

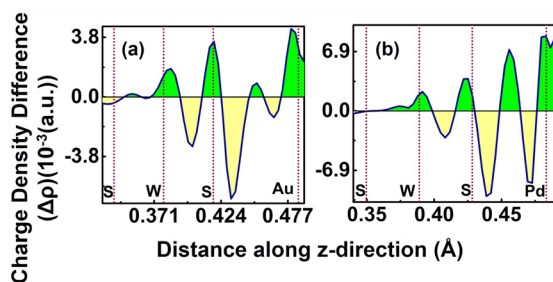


FIG. 5. 1D projection of average charge density difference along the  $z$ -direction for pure  $\text{WS}_2$  with (a) Au (b) Pd interface geometry. To study the charge transfer at the interface thoroughly, we show only single layer of gold atoms out of four. The relative positions of atoms are shown by the dotted lines along the  $y$  axis. The filled green area indicates the accumulation region, and the yellow indicates the depletion region. The values on the  $y$ -axis show that the charge accumulation in Pd is nearly double as compared to Au.

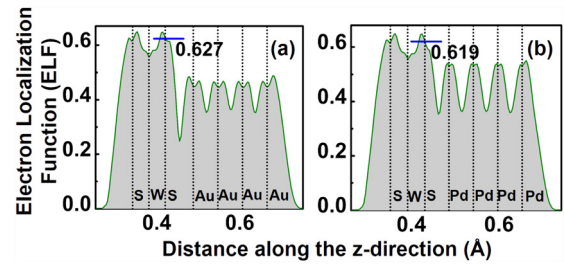


FIG. 6. 1D projection of average electron localization function along the  $z$ -direction of pure  $\text{WS}_2$  with (a) Au and (b) Pd contact. The position of atoms is shown by black dotted lines along the  $y$ -axis. The blue line indicates the value of ELF of the nearest sulfur atom in the  $\text{WS}_2$  monolayer.

is defined as the possibility of finding an electron in the neighborhood of a reference electron. Its value ranges from  $0 < \text{ELF} < 1$ , with the maximum limit  $\text{ELF} = 1$  corresponding to a perfect localization and  $\text{ELF} = 0.5$  corresponding to an electron-gas like pair probability.<sup>28</sup> Figure 6 shows the value of ELF for the  $\text{WS}_2$ -Au and  $\text{WS}_2$ -Pd interface. The value obtained for Pd is less when compared to Au. This implies that Au is more localized than Pd, indicating a better bonding for the  $\text{WS}_2$ -Pd interface.

It is interesting to note that for TMD channel based transistors, in a top contact device structure, two types of interfaces exist. One interface is between the TMD-metal and the other is between the TMD underneath the metal contact and TMD forming the channel.<sup>18</sup> Here, we find the SBH formed at the first interface. For calculating the SBH at the second interface, transport simulations need to be conducted along the device length. The effective SBH combining both the interfaces can then be determined using LDOS distribution. However, carrying transport simulations employing pseudopotentials with basis functions having higher orbital contribution requires a powerful computing system, as the number of atoms increases manifold from the bulk-configuration to device-configuration. Nevertheless, while discussing SBH and the associated contact resistance in the context of ON current of the MOSFET, the gate current is kept high, and the channel is inverted. In this condition, the CBM of the TMD channel region (not touching the metal) can be assumed to be lower than the CBM of the other TMD regime. Hence, the SBH evaluated in this work can be considered as the effective SBH.

In the above study, we investigate the contact nature of the pure and Cl doped monolayer  $\text{WS}_2$  with Au  $\langle 111 \rangle$  and Pd  $\langle 111 \rangle$ . First, the electronic structures of pure and doped supercells are investigated. We find that the band energies near to the conduction band edge align close to Fermi level with the formation of midgap states and band splitting. Further, the pure and doped optimized supercell are adsorbed on the metals. The interface with pure supercell determines that Au is physisorbed with  $\text{WS}_2$  and has an n-type SBH while Pd is chemisorbed with  $\text{WS}_2$  having a p-type SBH. Adsorption with the Cl doped supercell shows a reduction in the n-type SBH for both the metals. All the results are validated by studying charge redistribution at the  $\text{WS}_2$ -metal interface. The above understanding may further contribute to explore other TMD-metal interfaces, as well as in investigating various possible dopants for chalcogenide substitution.

The work was supported by Science Engineering and Research Board—Department of Science and Technology (SERB DST), Government of India, under Grant No. SR/S3/EECE/0151/2012. The authors would like to thank Quantum wise support staff for their useful discussions.

- <sup>1</sup>B. Radisavljevic, A. Radenovic, J. Brivio, V. Giacometti, and A. Kis, “Single-layer MoS<sub>2</sub> transistors,” *Nat. Nanotechnol.* **6**, 147–150 (2011).
- <sup>2</sup>W. Sik Hwang, M. Remskar, R. Yan, V. Protasenko, K. Tahy, S. Doo Chae, P. Zhao, A. Konar, H. (Grace) Xing, A. Seabaugh, and D. Jena, “Transistors with chemically synthesized layered semiconductor WS<sub>2</sub> exhibiting 105 room temperature modulation and ambipolar behavior,” *Appl. Phys. Lett.* **101**, 013107 (2012).
- <sup>3</sup>X. Liu, J. Hu, C. Yue, N. D. Fera, Y. Ling, Z. Mao, and J. Wei, “High performance field-effect transistor based on multilayer tungsten disulfide,” *ACS Nano* **8**, 10396–10402 (2014).
- <sup>4</sup>S. Das and J. Appenzeller, “WSe<sub>2</sub> field effect transistors with enhanced ambipolar characteristics,” *Appl. Phys. Lett.* **103**, 103501 (2013).
- <sup>5</sup>S. Larentis, B. Fallahzad, and E. Tutuc, “Field-effect transistors and intrinsic mobility in ultra-thin MoSe<sub>2</sub> layers,” *Appl. Phys. Lett.* **101**, 223104 (2012).
- <sup>6</sup>N. R. Pradhan, D. Rhodes, S. Feng, Y. Xin, S. Memaran, B.-H. Moon, H. Terrones, M. Terrones, and L. Balicas, “Field-effect transistors based on few-layered  $\alpha$ -MoTe<sub>2</sub>,” *ACS Nano* **8**, 5911–5920 (2014).
- <sup>7</sup>W. S. Leong, X. Luo, Y. Li, K. H. Khoo, S. Y. Quek, and J. T. Thong, “Low resistance metal contacts to MoS<sub>2</sub> devices with nickel-etched-graphene electrodes,” *ACS Nano* **9**, 869–877 (2014).
- <sup>8</sup>A. Chanana and S. Mahapatra, “Theoretical insights to niobium-doped monolayer MoS<sub>2</sub> gold contact,” *IEEE Trans. Electron Devices* **62**, 2346–2351 (2015).
- <sup>9</sup>S. Das, H.-Y. Chen, A. V. Penumatcha, and J. Appenzeller, “High performance multilayer MoS<sub>2</sub> transistors with scandium contacts,” *Nano Lett.* **13**, 100–105 (2013).
- <sup>10</sup>J. Kang, W. Liu, and K. Banerjee, “High-performance MoS<sub>2</sub> transistors with low-resistance molybdenum contacts,” *Appl. Phys. Lett.* **104**, 093106 (2014).
- <sup>11</sup>M. R. Laskar, D. N. Nath, L. Ma, E. W. Lee II, C. H. Lee, T. Kent, Z. Yang, R. Mishra, M. A. Roldan, J.-C. Idrobo *et al.*, “P-type doping of MoS<sub>2</sub> thin films using Nb,” *Appl. Phys. Lett.* **104**, 092104 (2014).
- <sup>12</sup>J. Suh, T.-E. Park, D.-Y. Lin, D. Fu, J. Park, H. J. Jung, Y. Chen, C. Ko, C. Jang, Y. Sun, R. Sinclair, J. Chang, S. Tongay, and J. Wu, “Doping against the native propensity of MoS<sub>2</sub>: Degenerate hole doping by cation substitution,” *Nano Lett.* **14**, 6976–6982 (2014).
- <sup>13</sup>L. Liu, S. Bala Kumar, Y. Ouyang, and J. Guo, “Performance limits of monolayer transition metal dichalcogenide transistors,” *IEEE Trans. Electron Devices* **58**, 3042–3047 (2011).
- <sup>14</sup>L. Yang, K. Majumdar, H. Liu, Y. Du, H. Wu, M. Hatzistergos, P. Y. Hung, R. Tieckelmann, W. Tsai, C. Hobbs, and P. D. Ye, “Chloride molecular doping technique on 2D materials: WS<sub>2</sub> and MoS<sub>2</sub>,” *Nano Lett.* **14**, 6275–6280 (2014).
- <sup>15</sup>P. A. Khomyakov, G. Giovannetti, P. C. Rusu, G. Brocks, J. van den Brink, and P. J. Kelly, “First-principles study of the interaction and charge transfer between graphene and metals,” *Phys. Rev. B* **79**, 195425 (2009).
- <sup>16</sup>C. Gong, G. Lee, B. Shan, E. M. Vogel, R. M. Wallace, and K. Cho, “First-principles study of metal-graphene interfaces,” *J. Appl. Phys.* **108**, 123711 (2010).
- <sup>17</sup>I. Popov, G. Seifert, and D. Tománek, “Designing electrical contacts to MoS<sub>2</sub> monolayers: A computational study,” *Phys. Rev. Lett.* **108**, 156802 (2012).
- <sup>18</sup>J. Kang, W. Liu, D. Sarkar, D. Jena, and K. Banerjee, “Computational study of metal contacts to monolayer transition-metal dichalcogenide semiconductors,” *Phys. Rev. X* **4**, 031005 (2014).
- <sup>19</sup>See <http://quantumwise.com/> for Atomistix ToolKit v.15.beta Quantumwise.
- <sup>20</sup>J. P. Perdew and A. Zunger, “Self-interaction correction to density-functional approximations for many-electron systems,” *Phys. Rev. B* **23**, 5048–5079 (1981).
- <sup>21</sup>C. Hartwigsen, S. Goedecker, and J. Hutter, “Relativistic separable dual-space Gaussian pseudopotentials from H to Rn,” *Phys. Rev. B* **58**, 3641–3662 (1998).
- <sup>22</sup>H. J. Monkhorst and J. D. Pack, “Special points for Brillouin-zone integrations,” *Phys. Rev. B* **13**, 5188 (1976).
- <sup>23</sup>H. Jiang, “Electronic band structures of molybdenum and tungsten dichalcogenides by the gw approach,” *J. Phys. Chem. C* **116**, 7664–7671 (2012).
- <sup>24</sup>A. Kumar and P. Ahluwalia, “Electronic structure of transition metal dichalcogenides monolayers 1H-MX<sub>2</sub> (M = Mo, W; X = S, Se, Te) from *ab-initio* theory: new direct band gap semiconductors,” *Eur. Phys. J. B* **85**, 186 (2012).
- <sup>25</sup>K. Dolui, I. Rungger, C. Das Pemmaraju, and S. Sanvito, “Possible doping strategies for MoS<sub>2</sub> monolayers: An *ab initio* study,” *Phys. Rev. B* **88**, 075420 (2013).
- <sup>26</sup>C. G. Van de Walle and J. Neugebauer, “First-principles calculations for defects and impurities: Applications to III-nitrides,” *J. Appl. Phys.* **95**, 3851–3879 (2004).
- <sup>27</sup>C. Gong, L. Colombo, R. M. Wallace, and K. Cho, “The unusual mechanism of partial Fermi level pinning at metal–MoS<sub>2</sub> interfaces,” *Nano Lett.* **14**, 1714–1720 (2014).
- <sup>28</sup>A. D. Becke and K. E. Edgecombe, “A simple measure of electron localization in atomic and molecular systems,” *J. Chem. Phys.* **92**, 5397 (1990).